

Dynamically stable negative-energy states induced by spin-transfer torquesJ. S. Harms^{1,*}, A. Rückriegel² and R. A. Duine^{1,3}¹*Institute for Theoretical Physics, Utrecht University, 3584CC Utrecht, The Netherlands*²*Institut für Theoretische Physik, Universität Frankfurt, Max-von-Laue Strasse 1, 60438 Frankfurt, Germany*³*Department of Applied Physics, Eindhoven University of Technology, P.O. Box 513, 5600 MB Eindhoven, The Netherlands*

(Received 8 February 2021; accepted 22 March 2021; published 5 April 2021)

We investigate instabilities of the magnetic ground state in ferromagnetic metals that are induced by uniform electrical currents, and, in particular, go beyond previous analyses by including dipolar interactions. These instabilities arise from spin-transfer torques that lead to Doppler-shifted spin waves. For sufficiently large electrical currents, spin-wave excitations have negative energy with respect to the uniform magnetic ground state while remaining dynamically stable due to dissipative spin-transfer torques. Hence, the uniform magnetic ground state is energetically unstable but is not able to dynamically reach the new ground state. We estimate this to happen for current densities $j \gtrsim (1 - D/D_c)10^{13}$ A/m² in typical thin-film experiments, with D the Dzyaloshinskii-Moriya interaction constant, and D_c the Dzyaloshinskii-Moriya interaction that is required for spontaneous formation of spirals or skyrmions. The critical current density can be made arbitrarily small for ultrathin-film thicknesses at the order of nanometers due to surface and interlayer effects. From an analog gravity perspective, the stable negative-energy states are an essential ingredient to implement event horizons for magnons—the quanta of spin waves—giving rise to, e.g., Hawking radiation, and can be used to amplify spin waves in a so-called black-hole laser.

DOI: [10.1103/PhysRevB.103.144408](https://doi.org/10.1103/PhysRevB.103.144408)**I. INTRODUCTION**

Unruh's 1981 paper, "Experimental black hole evaporation" [1], proposed that following the argument for thermal black-hole radiation [2], a sonic analog event horizon can be created by considering sound waves in a flowing medium. This sonic event horizon emits a thermal spectrum of sound waves and opens up possibilities for the experimental observation of Hawking radiation. The event horizon for sound waves is created by a transition from subsonic to supersonic background flow such that sound waves incoming from the subsonic region cannot escape the supersonic region once they have passed the event horizon. Motivated by Unruh's work, theoretical proposals of analog event horizons based on different systems were put forward [3–5]. These include phase oscillations in a Bose-Einstein condensate [6], slow light in dielectric media [7,8], trapped ion rings [9,10], Weyl semimetals [11], and as discussed in this article, metallic magnets [12]. Although Unruh's original proposal considers waves in water which cannot be pushed into the quantum regime, the existence of classically stimulated Hawking emission has been observed in Ref. [13]. Furthermore, thermal Hawking radiation in a Bose-Einstein condensate, a system which might be driven to the quantum regime, has been observed in Ref. [14].

Moreover, the combination of a black-hole and white-hole horizon—the time-reversed partner of a black-hole horizon—is proposed to lead to huge amplitude enhancements at specific resonant frequencies [15], thereby acting as a black-hole laser. The resonance frequencies occur due

to constructive interference of particle-hole coupling at each horizon, which gives rise to Hawking radiation in the quantum regime. An implementation of the latter is the spin-wave laser proposed in Ref. [16], which provides a way of injecting spin angular momentum into a magnetic sample through amplification of spin waves, driven by current induced spin-transfer torques [17].

Spin waves are collective excitations that occur in magnetically ordered systems and correspond, at the semiclassical level, to the precession of spatially separated spins where the phase difference between them is determined by the wavelength. Using spin waves for information transport and processing is the goal of magnonics [18]—the spin-wave analog of electronics. A difficulty towards realizing spin-wave-based technology is the finite lifetime of spin waves resulting from processes that lead to decay of spin angular momentum. The spin-wave laser gives a potential way to compensate relaxation of spin waves by injection of spin angular momentum.

In this article we investigate energetic and dynamic instabilities of spin waves in metallic ferromagnetic thin films induced by spin-transfer torques, i.e., torques arising from the interaction of the spin-polarized current and the magnetization dynamics [17,19–23]. More specifically, spin waves are Doppler shifted in the presence of an electrical current [21,24], with an effective spin-drift velocity proportional to the electrical current. This spin-wave Doppler shift was experimentally observed by Vlaminck and Bailleul [25]. The spin-drift velocity, if large enough, can lead to instabilities in the ferromagnetic ground state [21,23,26]. For the existence of analog horizons it is important to distinguish energetic and dynamic instabilities. Energetic instabilities are

*j.s.harms@uu.nl

characterized by the existence of negative-energy excitations, while dynamical instabilities lead to exponential growth of small-amplitude excitations. Contrary to most physical systems, these instabilities do not necessarily coincide for spin waves in a ferromagnetic metal due to dissipative spin-transfer torques [19]. We find that magnons—the quanta of spin waves—can be dynamically stable for a wide range of currents that make the ferromagnetic ground state energetically unstable.

In the context of analog gravity, the magnonic event horizon is defined by the transition from a region of positive-energy states to a region with dynamically stable negative-energy states. For linearly dispersing sound waves, such as waves in water, the negative-energy region corresponds to unidirectional movement of sound waves. In general, an event horizon is a region which couples positive-energy states to negative-energy states. For nonlinearly dispersing sound waves one can still define the event horizon as the region that couples positive-energy states and dynamically stable negative-energy states. These generalized event horizons are referred to as dispersive horizons [27].

The ferromagnetic thin-film setup we consider in this article is similar to Ref. [16] but treated more generally, including effects of surface and volume anisotropies, Dzyaloshinskii-Moriya interaction, dipole-dipole interactions, and finite thickness of the thin film. We find that the current density needed to create energetically unstable but dynamically stable states is of the order $j \gtrsim (1 - D/D_c)10^{13} \text{A/m}^2$ for typical thin-film experiments, with D the Dzyaloshinskii-Moriya constant and D_c the Dzyaloshinskii-Moriya interaction that is required for spontaneous formation of spirals or skyrmions. The critical current density can be made arbitrarily small for thin-film thicknesses of the order of a nanometer. This decrease is primarily due to the effects of surface anisotropy and interfacial Dzyaloshinskii-Moriya interaction.

The remainder of this article is organized as follows. We put forward our model and discuss spin-wave solutions in Sec. II. Furthermore, the critical current needed for energetic instabilities to exist and the region of dynamical stability are derived in Sec. III. Additionally, we derive the critical thickness at which the ferromagnetic ground state becomes unstable due to surface and interfacial effects in Appendix A. A derivation of the lowest energy dipole-exchange spin-wave mode is presented in Appendix B. We conclude with a Discussion and Outlook section.

II. METALLIC THIN-FILM FERROMAGNET

A. Model and setup

We consider a ferromagnetic metallic thin film of thickness L in the z direction with the surfaces corresponding to $z = \pm L/2$. We consider the setup in Fig. 1 that involves a thin film subject to a static external field \mathbf{H}_e applied in the y direction and a uniform charge current \mathbf{j} pointing in the $-x$ direction. For temperatures far below the Curie temperature, amplitude fluctuations in the magnetization are negligible. In this case the dynamics of the magnetization direction $\mathbf{n} = \mathbf{M}/M_s$ is described by the Landau-Lifshitz-Gilbert (LLG) equation, with spin-transfer torques (STTs), and Maxwell's equations in the

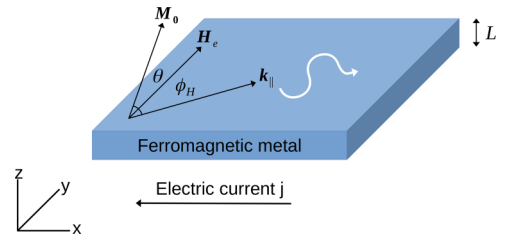


FIG. 1. Sketch of the setup. We consider a metallic ferromagnetic thin film of thickness L which is subjected to an external magnetic field \mathbf{H}_e pointing in the y direction and an electric current driven along the x direction. Furthermore, θ is the angle of the steady-state magnetization \mathbf{M}_0 with the plane and ϕ_H is the angle between the spin-wave propagation direction and the y axis.

magnetostatic limit. The LLG equation with STTs is given by [19]

$$(\partial_t + \mathbf{v}_s \cdot \nabla) \mathbf{n} = -\gamma \mathbf{n} \times \mathbf{H}_{\text{eff}} + \alpha \mathbf{n} \times \left(\partial_t + \frac{\beta}{\alpha} \mathbf{v}_s \cdot \nabla \right) \mathbf{n}, \quad (1)$$

provided that spin-orbit coupling is not very strong so that spin-orbit torques are negligible. Inclusion of spin-orbit torques in our discussion is straightforward but omitted here to reduce the number of parameters. In the above equation, the adiabatic spin-transfer torque is parametrized by the velocity $\mathbf{v}_s = -gP\mu_B \mathbf{j}/2eM_s$ that is referred to as spin-drift velocity, which is proportional to the current density \mathbf{j} . Here g is the Landé factor, μ_B the Bohr magneton, e the elementary charge, P the spin polarization of the current, and M_s the saturation magnetization. The LLG equation describes damped precession of the magnetization around the effective field $\mathbf{H}_{\text{eff}} = -\delta E/(M_s \delta \mathbf{n})$. Here, $E[\mathbf{n}]$ is the magnetic energy functional, which we consider to be of the general form

$$E = M_s \int dV \left\{ -\frac{1}{2} J \mathbf{n} \cdot \nabla^2 \mathbf{n} - \mu_0 \mathbf{H} \cdot \mathbf{n} - \frac{1}{2} K_v n_z^2 - \frac{1}{2} D [\hat{y} \cdot (\mathbf{n} \times \partial_x \mathbf{n}) - \hat{x} \cdot (\mathbf{n} \times \partial_y \mathbf{n})] \right\}. \quad (2)$$

In the above J is the spin stiffness, D the Dzyaloshinskii-Moriya interaction (DMI) constant that in this particular setup may result from interfacing the magnet with a heavy metal, and K_v is the volume anisotropy constant—this type of anisotropy is, e.g., typical in the Co-layer spin-wave spectroscopy experiments in Ref. [28]. The dimensionless parameters α and β characterize the strength of the Gilbert damping parameter and the nonadiabatic spin-transfer torques, respectively. Usually these dissipative constants are comparable, $\alpha \sim \beta$, and of the order 10^{-2} [29]. For now we neglect surface anisotropy in the energy functional, which we discuss in Appendix B. Additionally, dipole-dipole interactions are taken into account by considering the magnetostatic Maxwell's equations [30]

$$\nabla \times \mathbf{H} = \mathbf{j}, \quad \nabla \cdot \mathbf{B} = 0. \quad (3)$$

Here \mathbf{H} is the magnetic field strength and $\mathbf{B} = \mu_0(\mathbf{H} + \mathbf{M})$ the total magnetic field. In the steady state, the internal magnetic field \mathbf{H}_0 and the magnetization \mathbf{M}_0 are parallel. For an external magnetic field pointing in the y direction with $jL \ll 2H_e$, the

internal magnetic field and magnetization are related to the external magnetic field by

$$\mu_0 j_z \sin(\theta) \simeq (\mu_0 M_s - K_v) \sin(2\theta)/2 + \mu_0 H_e \sin(\theta), \quad (4)$$

with θ the angle between the magnetization direction and the x - y plane. We find that the steady-state magnetization points along the y axis if $K_v < \mu_0(H_e + M_s - jL/2)$, while the steady-state magnetization deviates from the y axis if $K_v > \mu_0(H_e + M_s - jL/2)$, where it acquires a component in the z direction. From this point onward we assume $K_v < \mu_0(H_e + M_s - jL/2)$ such that the steady-state magnetization is pointing in the y direction. Experimentally, this may be achieved by applying a sufficiently large external magnetic field.

B. Dipole-exchange spin-wave modes

The dipole-exchange spin-wave modes [28,31–38] are generated by dynamical fluctuations of both the magnetization direction and the demagnetizing field, which are small compared to \mathbf{M}_0 and \mathbf{H}_0 ,

$$\mathbf{M} = \mathbf{M}_0 + \mathbf{m}(t), \quad \mathbf{H} = \mathbf{H}_0 + \mathbf{h}_D(t). \quad (5)$$

Notice that up to linear order in the dynamical fluctuations, \mathbf{m} is perpendicular to \mathbf{M}_0 , lying in the x - z plane since we consider the magnitude of the magnetization to be constant $|\mathbf{M}| = M_s$. Both the static and dynamic part of the magnetization and magnetic field strength should satisfy the magnetostatic Maxwell equations (3). We accordingly require $\nabla \times \mathbf{h}_D = 0$, $\nabla \cdot \mathbf{b} = 0$, with $\mathbf{b} = \mu_0(\mathbf{h}_D + \mathbf{m})$. The first Maxwell equation allows us to write the dynamic demagnetizing field in terms of a scalar potential $\mathbf{h}_D = \nabla \Phi_D$. The second Maxwell equation accordingly gives $\nabla^2 \Phi_D = -\nabla \cdot \mathbf{m}$, where the magnetization \mathbf{m} outside the film is zero. The Landau-Lifshitz-Gilbert and magnetostatic Maxwell equations may

be rewritten by means of $\mathbf{n} \simeq \hat{z} \sqrt{2} \text{Re}[\Psi] + \hat{x} \sqrt{2} \text{Im}[\Psi] + \hat{y} (1 - |\Psi|^2)$, with the complex field $\Psi = (1/\sqrt{2})(\hat{z} + i\hat{x}) \cdot \mathbf{n}$. In these coordinates the linearized LLG and magnetostatic Maxwell equations become

$$\hat{\Omega} \Psi = -(\Omega_H - \Delta_v - \Lambda^2 \nabla^2) \Psi + \Delta_v \Psi^* + \frac{(\partial_z + i\partial_x)}{\sqrt{2}M_s} \Phi_D, \quad (6a)$$

$$\frac{\nabla^2 \Phi_D}{M_s^2} = \frac{(\partial_z - i\partial_x)}{\sqrt{2}M_s} \Psi + \frac{(\partial_z + i\partial_x)}{\sqrt{2}M_s} \Psi^*. \quad (6b)$$

Additionally, the exchange boundary conditions for thin films [39] require

$$\pm \partial_z \Psi - (K_s/J)(\Psi + \Psi^*) \Big|_{z=\pm L/2} = 0, \quad (7)$$

with K_s the surface anisotropy constant. In the above we defined the following dimensionless operators and variables [40]: dimensionless magnetic field $\Omega_H = \mu_0 H_e / \mu_0 M_s$, dimensionless volume anisotropy $\Delta_v = K_v / 2\mu_0 M_s$, exchange length $\Lambda = \sqrt{J/\mu_0 M_s}$, and the dimensionless frequency operator $\hat{\Omega} = i[(1 - i\alpha)\partial_t + (1 - i\beta)\mathbf{v}_s \cdot \nabla + \gamma D\partial_x]/(\gamma\mu_0 M_s)$.

Using the Bogoliubov ansatz and taking \mathbf{v}_s in the x direction, we write $\Psi(\mathbf{x}, t) = u(\mathbf{x})e^{-i\omega t} + v^*(\mathbf{x})e^{i\omega^* t}$ and $\Phi_D(\mathbf{x}, t) = w(\mathbf{x})e^{-i\omega t} + w^*(\mathbf{x})e^{i\omega^* t}$, where $(u(\mathbf{x}), v(\mathbf{x}), w(\mathbf{x})) \propto e^{i\mathbf{k} \cdot \mathbf{r}_\parallel} (u(\mathbf{k}, z), v(\mathbf{k}, z), w(\mathbf{k}, z))$, with $\mathbf{k} = (k_x, k_y)$ and $\mathbf{r}_\parallel = (x, y)$. The above plane-wave ansatz gives rise to a spectrum of spin-wave solutions. The lowest energy dipole-exchange spin-wave dispersion relation is obtained in Appendix B for thin films with thicknesses comparable to the exchange length $L \sim \mathcal{O}(\Lambda)$. Up to linear order in α and β , the lowest energy dipole-exchange spin-wave dispersion relation is given by

$$(\omega_{\mathbf{k}} - v_s k_x) \simeq \omega_{\mathbf{k}}^0 - i\kappa \alpha \omega_{\mathbf{k}}^0 - i\kappa(\alpha - \beta)v_s k_x, \quad (8)$$

where

$$(\omega_{\mathbf{k}}^0 - \gamma D k_x)/(\gamma\mu_0 M_s) = \sqrt{[\Omega_H - \Delta + \Lambda^2 k^2 - 1/2 \cos^2(\phi_H) f(k)]^2 - [\Delta + 1/2\{1 + \sin^2(\phi_H)\} f(k)]^2} \quad (9)$$

is the real part of the dispersion in the absence of an electrical current, which is plotted in Fig. 2. Here $f(k) = 1 - (1 - e^{-kL})/kL$ is the form factor, ϕ_H the angle between the spin-wave propagation direction and the y axis, and $\Delta \equiv \Delta_v + \Delta_s - 1/2$, with $\Delta_s = (\Lambda/\mu_0 M_s L) K_s$ the dimensionless parameter corresponding to the sum of surface anisotropies [34,39]. In the above, κ is an overall factor of the imaginary part of the dispersion relation, stemming from the fact that the isotropic Gilbert damping only enters in the diagonal part of Eq. (6a). This term is not of importance for the stability analyses, since it remains positive in the region of interest. The precise form of κ can be found in Appendix B.

III. ENERGETIC AND DYNAMICAL SPIN-WAVE INSTABILITIES

Motivated by theoretical predictions of magnonic black-/white-hole horizons [12] and black-hole lasers [15,16], we investigate energetic and dynamic instabilities in the

spin-wave spectrum due to a spin-polarized electrical current [21], including effects of dipole-dipole interactions, volume and surface anisotropies, and DMI. A negative real part of the spin-wave dispersion relation, Eq. (8), indicates energetic instabilities, necessary for analog black-/white-hole setups [3–5]. Dynamical instabilities, on the other hand, are characterized by a positive imaginary part of the spin-wave dispersion relation and classically lead to an exponential growth of unstable modes. In contrast to most physical systems, these two types of instabilities do not necessarily coincide for the magnetization dynamics in a metallic magnetic system due to the dissipative spin-transfer torques characterized by the parameter β . Accordingly, we investigate the regime in which the system is energetically unstable but dynamically stable, see Fig. 3. From Eq. (8) we find that the system is dynamically stable if

$$|(\alpha - \beta)v_s k_x + \alpha \gamma D k_x| < \alpha(\gamma\mu_0 M_s)\Omega_{\mathbf{k}} \quad (10)$$

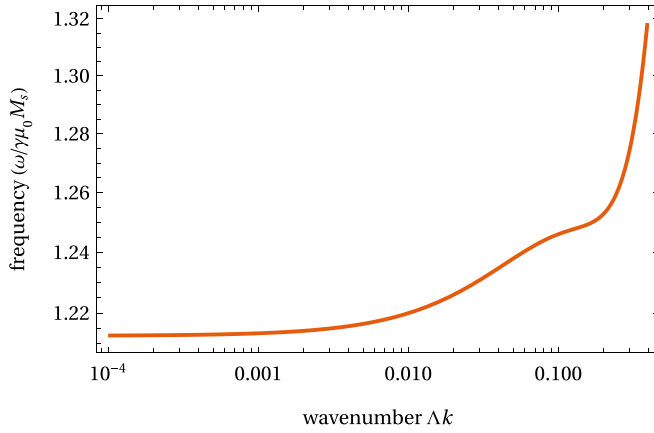


FIG. 2. Dispersion relation (9) of the lowest energy spin-wave mode including dipolar interactions and anisotropy. Here, we consider $\Omega_H = 1$, $D/\mu_0 M_s = 0$, $\Delta = -0.25$, $L \sim 40$ nm, and $\phi_H = \pi/2$.

is satisfied for all \mathbf{k} , with $\gamma \mu_0 M_s \Omega_{\mathbf{k}} = \omega_{\mathbf{k}}^0 - \gamma D k_x$ the inversion symmetric part of the dispersion relation (9). Energetic instabilities, on the other hand, are present if $\text{Re } \omega_{\mathbf{k}} < 0$, for some \mathbf{k} . By considering minima of the dispersion relation we find the critical current above which energetic instabilities exist should satisfy $\partial_{k_c} \text{Re } \omega_{k_c}|_{v_s=v_c} = 0$ and $\text{Re } \omega_{k_c}|_{v_s=v_c} = 0$, for some k_c . Thus energetic instabilities are present for currents $v_s > v_c$ and do not exist for $v_s < v_c$, which characterizes the

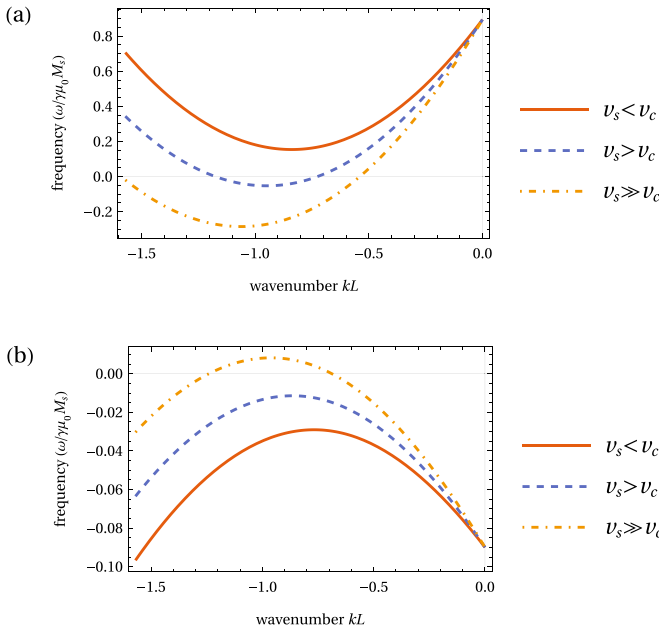


FIG. 3. Dispersion relation (8) for different values of the spin-drift velocity v_s , with $\alpha = 0.1$ and $\beta = 0.01$. (a) Real part of the dispersion relation. (b) Imaginary part of the dispersion relation. For small $v_s < v_c$, spin waves are energetically and dynamically stable (red). For spin-drift velocities larger than the critical velocity, $v_s > v_c$, we obtain energetically unstable but dynamically stable spin waves (blue). For very large $v_s \gg v_c$, spin waves are both energetically and dynamically unstable (yellow).

critical velocity v_c . The above constraints that determine the critical current are equivalent to

$$\partial_{k_c} \Omega_{k_c}^2 = 2\Omega_{k_c}^2/k_c, \quad (11a)$$

$$v_c/\gamma = [\mu_0 M_s / \sin(\phi_H)] \Omega_{k_c} / k_c - D. \quad (11b)$$

For spin waves traveling perpendicular to the external magnetic field, $\phi_H = \pi/2$ in Eq. (9), the constraint in Eq. (11a) is explicitly written as

$$[\Omega_H - \Delta]^2 - \Lambda^4 k_c^4 \sim [\Delta + f(k_c)][\Delta + f(k_c)^2], \quad (12)$$

where we used $f(k) - kf'(k) \sim f(k)^2$. We note that $f(k) \in [0, 1]$ and typically $\Delta = \Delta_v + \Delta_s - 1/2 \gtrsim -1/2$ with $\Omega_H \sim 1$. Accordingly, we assume $[\Delta + f(k_c)][\Delta + f(k_c)^2]/[\Omega_H - \Delta]^2$ to be small compared to unity around the critical wavelength k_c . Next, we expand $k_c^2 = \kappa_c^2 + \delta k_c^2$ around $\Lambda^2 \kappa_c^2 = \Omega_H - \Delta$, up to linear order in δk_c^2 and $[\Delta + f(k_c)][\Delta + f(k_c)^2]/[\Omega_H - \Delta]^2$ in Eq. (12). This gives

$$\Lambda^2 \delta k_c^2 \sim -\frac{1}{2} \frac{[\Delta + f(\kappa_c)][\Delta + f(\kappa_c)^2]}{\Omega_H - \Delta}. \quad (13)$$

Similarly, we find that Ω_{k_c} , up to first order in δk_c^2 and $[\Delta + f(k_c)]^2/[\Omega_H - \Delta]^2$, is given by

$$\Omega_{k_c} \sim 2[\Omega_H - \Delta] + \Lambda^2 \delta k_c^2 - \frac{1}{4} \frac{[\Delta + f(\kappa_c)]^2}{\Omega_H - \Delta}. \quad (14)$$

Finally, using Eq. (11b) we find that the critical current that generates energetic instabilities is up to linear order in δk_c^2 and $[\Delta + f(k_c)]^2/[\Omega_H - \Delta]^2$ given by

$$(v_c/\gamma \mu_0 M_s) \simeq \left(\frac{\Omega_{k_c}}{\kappa_c} \right) \left(1 - \frac{1}{2} \frac{\delta k_c^2}{\kappa_c^2} \right) - (D/\mu_0 M_s). \quad (15)$$

This can be rewritten as

$$v_c = \gamma(D_c - D), \quad (16)$$

where

$$(D_c/2\mu_0 M_s \Lambda) \simeq \sqrt{[\Omega_H - \Delta]^2 - (1/2)[\Delta + f(\kappa_c)]^2} \quad (17)$$

is the critical DMI constant above which the ground state becomes both energetically and dynamically unstable. Once DMI reaches this value, the homogeneous ground state becomes unstable. This results in the spontaneous formation of textures, typically spirals and skyrmions. Additionally, we note that the contribution of δk_c^2 drops out of the critical DMI, up to first order.

Finally, we find from Eq. (10) that the region in which electrical currents generate energetically unstable but dynamically stable spin waves is given by

$$\begin{cases} \gamma(D_c - D) < v_s < \gamma(D_c - D)|1 - \beta/\alpha|^{-1} & \beta < \alpha, \\ \gamma(D_c - D) < v_s < \gamma(D_c + D)|1 - \beta/\alpha|^{-1} & \beta > \alpha. \end{cases} \quad (18)$$

This provides a large window of stability, given that usually $\alpha \sim \beta$. We note that this region is determined by solely considering spin waves traveling along the x axis—perpendicular to the external magnetic field. This is a consequence of the fact that the critical current for energetic and dynamic instabilities increases as spin waves travel at increasing angles $|\phi_H - \pi/2|$ with respect to the x axis. In Fig. 4 we plotted the angular dependence of the critical current. Additionally, in the case

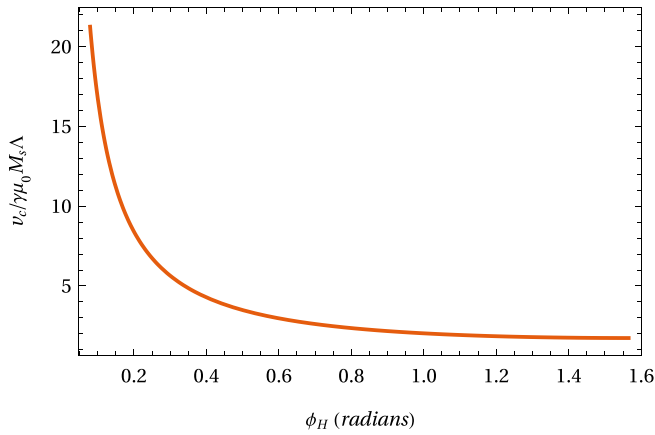


FIG. 4. Numeric solution of the dimensionless critical velocity $v_c/\gamma\mu_0M_s\Lambda$ in Eq. (11)—for dispersion relation (9)—against the angle ϕ_H in radians. We took the typical values $\Omega_H \sim 1$, $DL/\mu_0M_s\Lambda \sim 0.1$, $\Delta_v = K_v/2\mu_0M_s \sim 0.2$, $\Delta_s L = K_s/\mu_0M_s\Lambda \sim 0.4$, and $L/\Lambda = 3$.

where $\beta/\alpha > 2$ it is possible to have dynamically unstable but energetically stable states. This occurs when the right-hand side of Eq. (18) becomes smaller than the left-hand side. As a consequence, the DMI should be at least $D > D_c(1 - 2\alpha/\beta)$ for energetically unstable but dynamically stable states to exist in the region where $\beta/\alpha > 2$. Therefore, dynamically stable negative-energy states are difficult to create in materials when $\beta \gg \alpha$. For instance, in Ref. [41] a value of $\beta \sim 5\alpha$ was found.

Taking typical values for the saturation magnetization $\mu_0M_s \sim \mu_0H_e \sim 1$ T, gyromagnetic ratio $\gamma/2\pi \sim 30$ GHz T^{-1} , and exchange length $\Lambda = \sqrt{J/\mu_0M_s} \sim 5$ nm, we find the typical order of magnitude of the critical current $j_c \sim M_s|e|v_c/\mu_b \sim 10^{13}$ A/m², where we took $g \sim P \sim 1$, $M_s/\mu_B \sim 10^2$ nm⁻³, and $v_c \sim \gamma\mu_0M_s\Lambda \sim 10^3$ m/s. Furthermore, for typical values of DMI $DL/\mu_0M_s\Lambda^2 \sim 0.1$ [28,42,43], anisotropies $\Delta_v = K_v/2\mu_0M_s \sim 0.2$ and $\Delta_s L/\Lambda = K_s/\mu_0M_s\Lambda \sim 0.4$ [28,34], we find the critical current that is needed to create energetic instabilities, given in Eq. (16), is significantly reduced in thin films having thicknesses of a few nanometers, as is shown in Fig. 5. This reduction of the critical current is primarily due to the cumulative effect of DMI and surface anisotropies, which become prominent in ultrathin films as a consequence of their inverse scaling with respect to the thickness of the thin film.

IV. DISCUSSION AND OUTLOOK

We have investigated the occurrence of energetically unstable but dynamically stable spin-wave excitations due to spin-transfer torques, including effects of dipole-dipole interactions, anisotropies, and DMI. We have shown that in typical thin-film experiments [25,28,34], the critical current needed to create energetically unstable but dynamically stable states is of the order $j \gtrsim (1 - D/D_c)10^{13}$ A/m². If one could experimentally enhance the DMI to be near the critical DMI, above which the homogeneous ground state becomes unstable towards the formation of textures, such as spirals and skyrmions, then a relatively small current should be

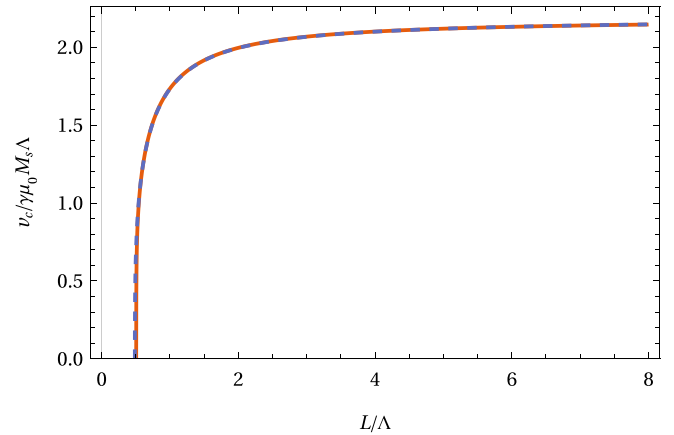


FIG. 5. Dimensionless critical velocity $v_c/\gamma\mu_0M_s\Lambda$ against dimensionless thickness L/Λ , taking typical values $\Omega_H \sim 1$, $DL/\mu_0M_s\Lambda^2 \sim 0.1$, $\Delta_v = K_v/2\mu_0M_s \sim 0.2$, $\Delta_s L/\Lambda = K_s/\mu_0M_s\Lambda \sim 0.4$. The dashed line corresponds to the linear approximation in Eq. (16), and the solid line corresponds to the numerically obtained solution of (11) with dispersion relation (9).

sufficient to create the dynamically stable negative-energy states. Additionally, we found that the critical current density becomes arbitrarily small for thin-film thicknesses of the order of nanometers. This decrease is primarily due to the cumulative effect of DMI and surface anisotropies, which become dominant in ultrathin films.

Furthermore, the region in which dynamically stable negative-energy spin-wave excitations exist is found to be large, given that typically $\alpha \sim \beta$. In the case where $\beta \gg \alpha$ we note that energetically stable, dynamically unstable states could occur. Hence, dynamically stable negative-energy states are difficult to create in materials when $\beta \gg \alpha$.

For the typical values considered in Sec. III, we see a slight deviation of the first-order critical velocity with respect to the numerical critical velocity at ultrathin-film thicknesses, see Fig. 5. This is due to the surface anisotropy contribution becoming larger in the ultrathin film limit, where the increased inaccuracy stems from the fact that we determine the critical velocity in Eq. (16) up to first order assuming $[\Delta + f(k_c)][\Delta + f(k_c)^2]$ and $[\Delta + f(k_c)]^2/2$ to be small compared to $[\Omega_H - \Delta]^2$. This approximation is accurate when anisotropies are small compared to the external magnetic field but describes the critical velocity less accurately when anisotropies become relatively large—especially volume anisotropy—approaching $2\Delta_v \lesssim \Omega_H + 1$. Additionally, the critical momentum k_c becomes small for ultrathin film thicknesses—if surface anisotropies are dominating—which makes the expansion of $1/k_c$ less accurate in this range. When dealing with relatively large anisotropies, it is more appropriate to expand the k_c^2 around $\kappa_c^2 = \sqrt{[\Omega_H - \Delta]^2 - [\Delta_v + \Delta_s]^2}$ in Eq. (12). In this case the critical DMI constant is given by $(D_c/\sqrt{2}\mu_0M_s) \simeq \sqrt{(\Omega_H - \Delta + \kappa_c^2)^2 - \tilde{f}(\Delta_v + \Delta_s + \tilde{f})/\kappa_c^2}$, with $\tilde{f} = f(\kappa_c) - 1/2$.

Finally energetically unstable, dynamically stable excitations are necessary to create analog black/white holes with

spin waves [3–5,12]. Furthermore, the combination of a black- and white-hole horizon is predicted to amplify spin waves of specific frequencies, giving rise to a spin-wave laser/amplifier [15,16]. Future research could investigate energetic and dynamic instabilities in antiferromagnetic metals. Additionally, this model could be used to compute the resonance frequencies of the spin-wave laser in Ref. [16] more realistically. Moreover, one could investigate nonlinear effects in such a setup, since nonlinear effects quickly become important around the resonance frequencies. The nonlinear regime could be investigated by means of the stochastic Landau-Lifshitz-Gilbert equation.

ACKNOWLEDGMENTS

This work is part of the research programme Fluid Spintronics with Project No. 182.069, which is (partly) financed by the Dutch Research Council (NWO). R.D. is a member of the D-ITP consortium, a program of the Dutch Organization for Scientific Research (NWO), which is funded by the Dutch Ministry of Education, Culture and Science (OCW).

APPENDIX A: CRITICAL THICKNESS OF ENERGETIC INSTABILITIES AT ZERO CURRENT

In this Appendix we determine the critical thickness at which spin-wave excitations become energetically unstable at zero electrical current. These energetic instabilities are due the increase in magnitude of surface anisotropies and DMI in the ultrathin-film limit and are dynamically unstable by Eq. (10). Additionally, the range of electrical currents that generates energetically unstable but dynamically stable spin-wave excitations decreases when approaching the critical thickness. This is a direct consequence of decreasing the critical current, see Sec. III. If surface anisotropies are dominant at small thicknesses, the critical thickness at which instabilities appear, at zero current and vanishing DMI, may be approximated at zeroth order by closing the spin-wave gap in Eq. (9), giving

$$\Omega_H - 2\Delta_0 \equiv \Omega_H + 1 - 2\Delta_v - 2\Delta_s^*/L_0 \sim 0, \quad (\text{A1})$$

with $k_c L \ll 1$ and $\Delta_s^* = \Delta_s L$ constant. For nonvanishing DMI, up to first order in $f(\kappa_c) \sim \kappa_c L/2 \ll 1$, we find that Eq. (11) is equivalent to

$$[\Omega_H - \Delta]^2 \sim [\Delta + f(k_c)]\Delta, \quad (\text{A2})$$

$$k_c [2(\Omega_H - \Delta) - (D^*/L)^2] \sim [\Delta + f(k_c)]f'(k_c), \quad (\text{A3})$$

where $D^* = (D/\mu_0 M_s \Delta)L$ is constant. We expand the above equations around $\Delta = \Delta_0 + \delta\Delta$, with $\delta\Delta = -(\Delta_s^*/L_0^2)\delta L + \mathcal{O}(\delta L^2)$. Up to first order Eq. (A2) gives

$$k_c L_0/2 \sim -4\delta\Delta. \quad (\text{A4})$$

We find that Eq. (A3) in combination with the above equation leads to

$$\delta L \sim \frac{\Omega_H L_0^2}{32\Delta_s^*} \left/ \left\{ \Omega_H \left[\frac{1}{L_0^2} + \frac{1}{6} - \frac{L_0}{32\Delta_s^*} \right] - \frac{3}{16} - \left(\frac{D^*}{L_0^2} \right)^2 \right\} \right., \quad (\text{A5})$$

with $L_0 = 2\Delta_s^*/(2\Omega_H + 1 - 2\Delta_v)$ given by Eq. (A1). We thus find that the critical thickness for spin-wave instabilities is

given by $L \sim L_0 + \delta L$, in the case that surface anisotropies dominate in the ultrathin film.

APPENDIX B: APPROXIMATE DIPOLE-EXCHANGE MODE IN THIN FILMS

Here we discuss an analytic approximation of the lowest energy spin-wave dispersion relation for the setup discussed in Sec. II, using the thin-film magnetostatic Green's function [33,34,37,38,44]. We start by expressing the demagnetizing field \mathbf{h}_D in Eqs. (5), (6a), (6b) in terms of the magnetization by using the magnetostatic Green's function. It is explicitly given by

$$\mathbf{h}_D(\mathbf{k}, z) = \int_{-L/2}^{L/2} dz' \mathbf{G}(\mathbf{k}; z - z') \mathbf{m}(\mathbf{k}; z'), \quad (\text{B1})$$

where the magnetostatic Green's function [37,44] satisfies the magnetostatic Maxwell equation, Eq. (6b), along with the appropriate boundary conditions [45]. It is explicitly given by

$$G_{\hat{\xi}\hat{\eta}\hat{z}}(k; z, z') = \begin{pmatrix} -G_p & 0 & iG_q \\ 0 & 0 & 0 \\ iG_q & 0 & G_p - \delta(z - z') \end{pmatrix}, \quad (\text{B2})$$

with $\hat{\xi} \propto \mathbf{k}$ the in-plane direction of spin-wave propagation, $\hat{\eta}$ the orthogonal in-plane direction, \hat{z} the thickness direction, $G_p = \frac{|k|}{2} \exp(-|k||z - z'|)$, and $G_q = G_p \text{sgn}(z - z')$. By substituting Eq. (B1) into the linearized Landau-Lifshitz-Gilbert equation, Eq. (6a), we obtain the effective linearized LLG equation,

$$\hat{\Omega}\Psi = -[\Omega_H - \Delta_{v/s} - \Lambda^2 \nabla^2]\Psi + \Delta_{v/s}\Psi^* + \int_{-L/2}^{L/2} \frac{1}{2} [A_k \Psi_k + B_k \Psi_{-k}] dz', \quad (\text{B3})$$

where $A_k = \cos^2(\phi_H)G_p - \delta(z - z')$, $B_k = \{1 + \sin^2(\phi_H)\}G_p - 2\sin(\phi_H)G_q - \delta(z - z')$, and ϕ_H the angle between wave vector \mathbf{k} and the y axis. Additionally, we introduced the dimensionless anisotropy constant $\Delta_{v/s} = K_{v/s}/2\mu_0 M_s$, where we took $K_{v/s} = K_v + K_s^- \delta(z - L/2) + K_s^+ \delta(z + L/2)$. Here K_s corresponds to the surface anisotropies of the thin film. Following Gladii *et al.* [34], we add the term $(K_s^\pm/2)\delta(z \pm L/2)n_z^2$ in the energy functional Eq. (2) to account for surface anisotropies. This differs from the approach used by Kalinikos and Slavin [38], where surface anisotropies determine the exchange boundary conditions of the thin film [39].

Using the Bogoliubov ansatz $\Psi(\mathbf{x}, t) = u(\mathbf{x})e^{-i\omega t} + v^*(\mathbf{x})e^{i\omega^* t}$, with $(u(\mathbf{x}), v(\mathbf{x})) = \int \frac{d^2\mathbf{k}}{2\pi} e^{i\mathbf{k}\cdot\mathbf{r}} (u(\mathbf{k}, z), v(\mathbf{k}, z))$, the linearized LLG equation becomes

$$\begin{pmatrix} \hat{F} + 1/2 & 1/2 - \Delta_{v/s} \\ \Delta_{v/s} - 1/2 & -\hat{F}^* - 1/2 \end{pmatrix} \begin{pmatrix} u(k, z) \\ v(k, z) \end{pmatrix} + \int_{-L/2}^{L/2} dz' \begin{pmatrix} -C(s) & D^+(s) \\ -D^-(s) & C(s) \end{pmatrix} \begin{pmatrix} u(k, z') \\ v(k, z') \end{pmatrix} = 0, \quad (\text{B4})$$

with $s = z - z'$, $\hat{F} = \Omega + (\Omega_H - \Delta_v + \Lambda^2 k^2 - \Lambda^2 \partial_z^2)$, $\hat{F}^* = -\Omega^* + (\Omega_H - \Delta_v + \Lambda^2 k^2 - \Lambda^2 \partial_z^2)$, $C(s) = (1/2) \cos^2(\phi_\xi) G_p$, and $D^\pm(s) = -(1/2) \{1 + \sin^2(\phi_\xi)\} G_p \pm |\sin(\phi_\xi)| G_q$.

Furthermore, $\gamma\mu_0M_s\Omega = (1 + i\alpha)\omega + (1 + i\beta)v_s k_x + \gamma Dk_x$ and $\gamma\mu_0M_s\Omega^* = (1 - i\alpha)\omega + (1 - i\beta)v_s k_x + \gamma Dk_x$.

The magnetization profile in the thickness direction may be expanded in eigenfunctions of the unpinned exchange boundary conditions, which form a complete basis [37]. We approximate the magnetization profile of the lowest mode by the lowest Fourier mode, for thicknesses of the order $L \sim \mathcal{O}(\Lambda)$,

$$\begin{pmatrix} u(k, z) \\ v(k, z) \end{pmatrix} \sim u^0(k) \sqrt{\frac{1}{L}} \begin{pmatrix} 1 \\ 0 \end{pmatrix} + v^0(k) \sqrt{\frac{1}{L}} \begin{pmatrix} 0 \\ 1 \end{pmatrix}, \quad (\text{B5})$$

which is the uniform-mode approximation. Using the above ansatz, the linearized LLG equation, Eq. (B4), becomes

$$\begin{pmatrix} \Omega + \Omega_d & -\Omega_i \\ \Omega_i & \Omega^* - \Omega_d \end{pmatrix} = 0, \quad (\text{B6})$$

where

$$\Omega_d = \Omega_H - \Delta + \Lambda^2 k^2 - 1/2 \cos^2(\phi_H) f(k), \quad (\text{B7a})$$

$$\Omega_i = \Delta + 1/2 \{1 + \sin^2(\phi_H)\} f(k). \quad (\text{B7b})$$

With $f(k) = 1 - (1 - e^{-kL})/kL$, $\Delta = \Delta_v + \Delta_s - 1/2$ and $\Delta_s = (\Lambda/2\mu_0M_sL)(K_s^- + K_s^+)$. Hence, the lowest mode dispersion relation, up to first order in α and β , is given by

$$(\omega_{\mathbf{k}} - v_s k_x) \simeq \omega_{\mathbf{k}}^0 - i\kappa\alpha\omega_{\mathbf{k}}^0 - i\kappa(\alpha - \beta)v_s k_x, \quad (\text{B8})$$

with $(\omega_{\mathbf{k}}^0 - \gamma Dk_x)^2 / (\gamma\mu_0M_s)^2 = \Omega_{\mathbf{k}}^2$, $\kappa = (\Omega_d/\Omega_{\mathbf{k}})$ and

$$\Omega_{\mathbf{k}}^2 = [\Omega_H - \Delta + \Lambda^2 k^2 - 1/2 \cos^2(\phi_H) f(k)]^2 - [\Delta + 1/2 \{1 + \sin^2(\phi_H)\} f(k)]^2. \quad (\text{B9})$$

-
- [1] W. G. Unruh, *Phys. Rev. Lett.* **46**, 1351 (1981).
[2] S. W. Hawking, *Nature (London)* **248**, 30 (1974).
[3] *Analogue Gravity Phenomenology*, edited by D. Faccio, F. Belgiorno, S. Cacciatori, V. Gorini, S. Liberati, and U. Moschella, Lecture Notes in Physics Vol. 870 (Springer International Publishing, Cham, Switzerland, 2013).
[4] M. Novello, M. Visser, and G. Volovik, *Artificial Black Holes* (World Scientific, Singapore, 2002).
[5] C. Barcelo, S. Liberati, and M. Visser, *Living Rev. Relativity* **8**, 12 (2005).
[6] L. J. Garay, J. R. Anglin, J. I. Cirac, and P. Zoller, *Phys. Rev. Lett.* **85**, 4643 (2000).
[7] U. Leonhardt, *Phys. Rev. A* **62**, 012111 (2000).
[8] U. Leonhardt and P. Piwnicki, *Phys. Rev. Lett.* **84**, 822 (2000).
[9] B. Horstmann, B. Reznik, S. Fagnocchi, and J. I. Cirac, *Phys. Rev. Lett.* **104**, 250403 (2010).
[10] R. Schützhold, M. Uhlmann, L. Petersen, H. Schmitz, A. Friedenauer, and T. Schätz, *Phys. Rev. Lett.* **99**, 201301 (2007).
[11] G. E. Volovik, *JETP Lett.* **104**, 645 (2016).
[12] A. Roldán-Molina, A. S. Nunez, and R. A. Duine, *Phys. Rev. Lett.* **118**, 061301 (2017).
[13] S. Weinfurter, E. W. Tedford, M. C. J. Penrice, W. G. Unruh, and G. A. Lawrence, *Phys. Rev. Lett.* **106**, 021302 (2011).
[14] J. R. Muñoz de Nova, K. Golubkov, V. I. Kolobov, and J. Steinhauer, *Nature (London)* **569**, 688 (2019).
[15] S. Corley and T. Jacobson, *Phys. Rev. D* **59**, 124011 (1999).
[16] R. J. Doornenbal, A. Roldán-Molina, A. S. Nunez, and R. A. Duine, *Phys. Rev. Lett.* **122**, 037203 (2019).
[17] A. Brataas, A. D. Kent, and H. Ohno, *Nat. Mater.* **11**, 372 (2012).
[18] A. V. Chumak, V. I. Vasyuchka, A. A. Serga, and B. Hillebrands, *Nat. Phys.* **11**, 453 (2015).
[19] D. C. Ralph and M. D. Stiles, *J. Magn. Magn. Mater.* **320**, 1190 (2008).
[20] J. C. Slonczewski, *J. Magn. Magn. Mater.* **159**, L1 (1996).
[21] J. Fernández-Rossier, M. Braun, A. S. Núñez, and A. H. MacDonald, *Phys. Rev. B* **69**, 174412 (2004).
[22] R. A. Duine, A. S. Núñez, J. Sinova, and A. H. MacDonald, *Phys. Rev. B* **75**, 214420 (2007).
[23] G. Tatara and H. Kohno, *Phys. Rev. Lett.* **92**, 086601 (2004).
[24] Y. B. Bazaliy, B. A. Jones, and S.-C. Zhang, *Phys. Rev. B* **57**, R3213(R) (1998).
[25] V. Vlamincck and M. Bailleul, *Science* **322**, 410 (2008).
[26] J. Shibata, G. Tatara, and H. Kohno, *Phys. Rev. Lett.* **94**, 076601 (2005).
[27] J. Chaline, G. Jannes, P. Maïssa, and G. Rousseaux, *Lect. Notes Phys.* **870**, 145 (2013).
[28] J. Lucassen, C. F. Schippers, M. A. Verheijen, P. Fritsch, E. J. Geluk, B. Barcones, R. A. Duine, S. Wurmehl, H. J. M. Swagten, B. Koopmans, and R. Lavrijsen, *Phys. Rev. B* **101**, 064432 (2020).
[29] Y. Tserkovnyak, H. J. Skadsem, A. Brataas, and G. E. W. Bauer, *Phys. Rev. B* **74**, 144405 (2006).
[30] R. Damon and J. Eshbach, *J. Phys. Chem. Solids* **19**, 308 (1961).
[31] A. Kreisel, F. Sauli, L. Bartosch, and P. Kopietz, *Eur. Phys. J. B* **71**, 59 (2009).
[32] S. M. Rezende, *Phys. Rev. B* **79**, 174411 (2009).
[33] M. Kostylev, *J. Appl. Phys.* **113**, 053907 (2013).
[34] O. Gladii, M. Haidar, Y. Henry, M. Kostylev, and M. Bailleul, *Phys. Rev. B* **93**, 054430 (2016).
[35] R. E. De Wames and T. Wolfram, *J. Appl. Phys.* **41**, 987 (1970).
[36] T. Wolfram and R. DeWames, *Prog. Surf. Sci.* **2**, 233 (1972).
[37] B. A. Kalinikos, *Sov. Phys. J.* **24**, 718 (1981).
[38] B. A. Kalinikos and A. N. Slavin, *J. Phys. C* **19**, 7013 (1986).
[39] R. F. Soohoo, *Phys. Rev.* **131**, 594 (1963).
[40] We neglected the contribution of the driving current \mathbf{j} to the magnetic field \mathbf{H} in Ω_H .
[41] J.-Y. Chauléau, H. G. Bauer, H. S. Körner, J. Stigloher, M. Härtinger, G. Woltersdorf, and C. H. Back, *Phys. Rev. B* **89**, 020403(R) (2014).
[42] M. Belméguenai, J.-P. Adam, Y. Roussigné, S. Eimer, T. Devolder, J.-V. Kim, S. M. Cherif, A. Stashkevich, and A. Thiaville, *Phys. Rev. B* **91**, 180405(R) (2015).
[43] A. A. Stashkevich, M. Belméguenai, Y. Roussigné, S. M. Cherif, M. Kostylev, M. Gabor, D. Lacour, C. Tiusan, and M. Hehn, *Phys. Rev. B* **91**, 214409 (2015).
[44] K. Y. Guslienko and A. N. Slavin, *J. Magn. Magn. Mater.* **323**, 2418 (2011).
[45] J. D. Jackson, *Classical Electrodynamics* (Wiley, New York, 1998).